Advances in Geo-Energy Research

Vol. 5, No. 1, p. 104-118, 2021

Original article

A multi-field coupling model of gas flow in fractured coal seam

Dayu Ye[1,2], Guannan Liu[1,2,3]*, Feng Gao[1,2,3], Rongguang Xu[4], Fengtian Yue[2,3]

[1]*State Key Laboratory for Geomechanics and Deep Underground Engineering, China University of Mining and Technology, Xuzhou 221116, P. R. China*

[2]*Mechanics and Civil Engineering Institute, China University of Mining and Technology, Xuzhou 221116, P. R. China*

[3]*Laboratory of Mine Cooling and Coal-heat Integrated Exploitation, China University of Mining and Technology, Xuzhou 221116, P. R. China*

[4]*Department of Mechanical and Aerospace Engineering, The George Washington University, Washington 20052, USA*

Keywords:
Fractal
coal permeability
gas sorption
coal microstructure
thermal conduction

Cited as:
Ye, D., Liu, G., Gao, F., Xu, R., Yue, F. A multi-field coupling model of gas flow in fractured coal seam. Advances in Geo-Energy Research, 2021, 5(1): 104-118, doi: 10.46690/ager.2021.01.10

Abstract:
The structure of fractures and pores has a dominant impact on the heat transfer-seepage-deformation process of a coal seam. Previous models have primarily used the cubic permeability model to characterize coal seam permeability properties. In this study, we developed a new multi-field coupling model, which includes fracture and pore structure, coal seam temperature, effective stress and gas seepage. Two major extraction scenarios were simulated: the unconstrained plane strain state and the uniaxial plane strain state. In addition, two microstructural parameters were applied to characterize coal permeability: the maximum fracture length and the fractal dimension for the fracture. The results show that the fractal seepage model provides a more realistic and reliable characterization of resource migration and extraction processes in unconventional reservoirs than the cubic-law permeability model. Compared with the cubic-law permeability model, the permeability calculated by the model proposed in this paper changes about 17.09%-91.56%. Furthermore, coal seam permeability is proportional to the maximum fracture length and the fractal dimension for the fracture. The permeability changes about 17.09% and 17.18% with the different fractal dimension, and about 87.17% and 91.56% with the different maximum fracture length. However, the fractal dimension and coal seam permeability are inversely proportional to seam temperature.

1. Introduction

Coal bed methane (CBM) is an essential part of the world's clean energy mix (Øren and Bakke, 2002). Fracture and pore structure are extremely complex, which is the key factor affecting the migration behavior of coalbed methane (Cai et al., 2017; Li et al., 2018; Zeng et al., 2020). In the process of CBM extraction, various factors affect the fracture and pore structure of a coal seam, such as gas adsorption-desorption, the thermal conductivity of the coal seam, the long-term effects of ground stress, and extruded deformation, which has an obvious impact on permeability (Arand and Hesser, 2017; Li et al., 2020; Liu et al., 2020). The contribution and evolution of coal seam microstructure in the migration and extraction of coalbed methane is thus of great theoretical and engineering significance (Barton and Hsieh, 1989; Kulatilake et al., 1995; Qin et al., 2019).

As an essential influence on the migration of CBM, thermal conduction in a reservoir initiates a variety of interactions, such as coal seam deformation, gas seepage and adsorption-desorption effects. Higher temperatures lead to a decrease in the Langmuir constant, causing a lower slope of the isotherm (Bustin and Clarkson, 1998). The adsorption of CBM has a significant negative correlation with coal seam temperature (Wang et al., 2018). Harpalani and Schraufnagel conclude that in percolation tests, the gas desorption effect due to temperature changes caused the contraction of the coal matrix, and consequently increased the permeability of the coal seam (Harpalani and Schraufnagel, 1990). Through simulations, Cai

Yandy Scientific Press

*Corresponding author.
E-mail address: theoye@cumt.edu.cn (D. Ye); guannanliu@cumt.edu.cn (G. Liu); fgao@cumt.edu.cn (F. Gao); xrg117@gwmail.gwu.edu (R. Xu); yueft@163.com (F. Yue).

Received February 25, 2021; revised March 8, 2021; accepted March 9, 2021; available online March 12, 2021.

et al. (2017) concluded that methane desorption clearly occurs at a high temperature, which enables a significant increase in coal seam permeability.

The quantitative study of the interaction of thermal conduction, seepage and adsorption-desorption during CBM extraction is a principal focus of current research. Current seepage studies considering various factors such as heat conduction, adsorption-desorption, and matrix deformation are usually based on Darcy's law (Liu et al., 2020). Mctigue developed a gas-saturated thermoelastic model and calculated the gas migration at a constant temperature (McTigue, 1986). Jafari and Babadagli characterized seepage properties through a derived non-linear multiple regression equation and defined equivalent permeability (Jafari and Babadagli, 2012). Cui and Bustin used the classical model to derive an expression for permeability that incorporates matrix stress and pore pressure (Cui and Bustin, 2005). However, previously published models, including those mentioned above, do not consider the effect of reservoir microstructure on fluid migration and extraction (Au et al., 2016; Liu et al., 2019; Wang et al., 2020). Further, in previous seepage studies involving the microstructure of the coal seam, the thermal effects have not been coupled to the models (Zhu et al., 2011; Ni et al., 2018).

In order to study the influence of the reservoir microstructure and thermal effects on gas migration, we developed a new fractal model to quantitatively analyze the contribution to the macroscopic seepage of the coal seam microstructure under thermal effects. The evolution of coal seam temperature, gas pressure, and coal seam deformation with the extraction process under thermal-hydraulic-mechanical interaction was studied. In addition, we analyzed the impact of coal microstructure on permeability, and studied the effect of the characteristic parameters on the microstructure.

2. Governing equations

As the predominant non-linear reservoir, coal seam has a complex pore-fracture structure. In order to quantify the effects of this complex structure, we coupled the microstructural parameters to the thermal-seepage model. This model includes the adsorption-desorption effects and the thermal-hydrological-mechanical interactions. Besides, the following assumptions were made to simplify the calculations (Palmer, 2009; Raeini et al., 2017):

1) Gas in pores is saturated;
2) Coal deformation meets linear elasticity;
3) Adsorption deformation is a small deformation;
4) The effects of heterogeneity and anisotropy are neglected.

2.1 Governing equations for coal seam

2.1.1 Equations for coal permeability

In this subsection, we develop a fractal-seepage model to analyze the microstructure of the coal seam. Based on this model, this paper studies the impacts of coal seam structure on macroscopic permeability. Miao states that the number of fractures whose lengths lie between l and $l+dl$ is (Yu et al., 2002; Miao et al., 2015):

$$-dN(l) = D_f l_{\max}^{D_f} l^{-(D_f+1)} dl \tag{1}$$

where D_f is the fracture fractal dimension, $l_{\max}$ is the maximum length for fractures and N is the number of fissures in a coal unit. Further, the fractal dimension for the fracture is expressed as (Yu and Li, 2001; Miao et al., 2015):

$$D_f = d_E + \frac{\ln \phi}{\ln \frac{l_{\min}}{l_{\max}}} \tag{2}$$

where d_E is the Euclid dimension, and $d_E = 2$ and 3 respectively in two and three dimensions. ϕ is the porosity of coal seam fracture, $l_{\min}$ and $l_{\max}$ represent the minimum and maximum fracture lengths in the coal seam unit, respectively, and in the case of the usual $0 < D_f < 2$, there is $l_{\min} << l_{\max}$. Miao derived the flow through the full fracture for the general cases as follows (Miao et al., 2015):

$$Q = \frac{\beta^3}{12\mu} \frac{D_f(1-\cos^2\gamma\sin^2\theta)}{4-D_f} \frac{\Delta p}{L_0} l_{\max}^4 \tag{3}$$

where $\beta = a/l$, a is the effective aperture, θ is the dip angle of a fracture, γ is the azimuth angle of a fracture, p is the pressure in fractures, and L_0 is the side length of a unit cell of fracture system. According to Darcy's law:

$$Q = \frac{kA_f}{\mu} \frac{\Delta p}{L_0} \tag{4}$$

where k is the permeability of the coal seam, A_f is the cross-sectional area of the characteristic unit of the fracture network. Combining Eqs. (1)-(4) as well as simplifying them, we obtain the governing equation for coal seam permeability as:

$$k = \frac{\beta^3}{12A_f} \frac{D_f(1-\cos^2\gamma\sin^2\theta)}{4-D_f} l_{\max}^4 \tag{5}$$

2.1.2 Equations for coal deformation

Changes in the temperature of the coal seam significantly affect the properties of the coal. This effect causes changes in porosity and matrix deformation. We therefore approximate the swelling/shrinkage of the coal seam as thermal swelling/shrinkage (Palmer and Mansoori, 1996). In this regard, the adsorption intrinsic relationship for coal bed methane at a gradual change in temperature is derived as (Zhu et al., 2011):

$$\sigma_{ij} = 2G\varepsilon_{ij} + \frac{2G\nu}{1-2\nu}\varepsilon_{kk}\delta_{ij} - \alpha p\delta_{ij} - K\alpha_T T\delta_{ij} - K\varepsilon_s\delta_{ij} \tag{6}$$

where G is the shear modulus, ν is Poisson's ratio, and δ_{ij} is Kronecker delta. $K = 2G(1+\nu)/3$ is the bulk modulus, and $(1-2\nu) = E/3(1-2\nu)$. α_T is the coefficient of thermal expansion of coal seam. $\alpha = 1 - K/K_s$ is Biot's coefficient, where K_s is the bulk modulus of coal. And $\varepsilon_s = \alpha_{sg}V_{sg}$ is the matrix shrinkage strain caused by the desorption, where V_{sg} is the content of absorbed gas. The deformation for the coal matrix can be derived from the assumptions (Zhang et al., 2008):

$$\sigma_{ij} + f_{ij} = 0 \tag{7}$$

where f_{ij} is the component of force, and σ_{ij} is the component of stress. Furthermore, according to the equation for the relationship between strain and stress:

$$\varepsilon_{ij} = \frac{1}{2}(u_{i,j} + u_{j,i}) \tag{8}$$

where ε_{ij} is the strain component in different directions. $u_{i,j}$ and $u_{j,i}$ are the components of the displacement. Substituting Eqs. (7) and (8) into Eq. (6):

$$Gu_{i,kk} + \frac{G}{1-2\mu}u_{k,ki} - \alpha p_{,i} - K\alpha_T T_{,i} - K\varepsilon_{s,i} + f_i = 0 \tag{9}$$

Eq. (9) is the matrix deformation equation of the coal seam contributed by thermal gradients, gas pressure effects, and adsorption-induced matrix strain. Further, the evolution of porosity could be caused by matrix deformation due to these factors. The porosity model with multifactorial effects is as follows (Zhu et al., 2011):

$$\phi = \alpha - (\alpha - \phi_0)\exp\left(\frac{\overline{\sigma}_0 - \overline{\sigma} + p_0 - p}{K}\right) \tag{10}$$

where ϕ_0 is the initial porosity with pressure p_0 and stress $\overline{\sigma_0}$, and the main stress $\overline{\sigma} = 1/3(\sigma_3 + \sigma_2 + \sigma_3)$.

2.2 Governing equations for methane

2.2.1 Equations for gas migration

According to the state of coalbed methane, the gas can be divided into free phase and adsorbed phase. The fractures are the main space for the transport and adsorption of the gas. The CBM in the various phases of the coal seam is (Zhu et al., 2011):

$$m = \rho_g\phi + \rho_{ga}\rho_c V_{sg} \tag{11}$$

where ρ_g is methane density, ρ_{ga} is the standard condition density, and ρ_c is the coal density. V_{sg} is the gas absorption volume, which can be defined as (Liang, 2000):

$$V_{sg} = \frac{V_L p}{p + P_L}\exp\left[-\frac{c_2}{1 + c_1 p}(T_{ar} + T - T_t)\right] \tag{12}$$

where P_L and V_L represent the Langmuir pressure and volume constant at T_t. T_t is the reference temperature, T_{ar} is the absolute reference temperature in the stress-free state, and c_1 and c_2 are the coefficients of pressure and temperature.

Combining Eqs. (11) and (12), Darcy's law, mass conservation of the gas, and the ideal gas equation, we can obtain:

$$\begin{aligned}\frac{R}{M_g}\frac{\partial m}{\partial t} &= \frac{\partial \phi}{\partial t}\frac{p}{T_{ar}+T} + \frac{\partial p}{\partial t}\frac{\phi}{T_{ar}+T} \\ &\quad - \frac{\partial T}{\partial t}\frac{\phi p}{(T_{ar}+T)^2} + \frac{p_a\rho_c V_L Y_1 Y_2}{T_a} \\ &\quad \times\left\{\left[\frac{c_2 c_1 Y_3}{(1+c_2 p)^2} + \frac{1}{(p+p_L)^2}\right]\frac{\partial p}{\partial t} - \frac{c_1}{1+c_1 p}\frac{\partial T}{\partial t}\right\}\end{aligned} \tag{13}$$

where $Y_1 = p_L/(p + p_L)$, $Y_2 = \exp[-c_2/(1 + c_2 p)(T_{ar} + T - T_t)]$, $Y_3 = (T_{ar} + T - T_t)$.

Additionally, based on Eq. (6), we can obtain the volume strain as follows (Zhu et al., 2011):

$$\varepsilon_v = \frac{1}{K}(\bar{\sigma} + \alpha p) + \alpha_T T + \varepsilon_s \tag{14}$$

The deformation of the coal seam due to adsorption is $\varepsilon_S = \alpha_{sg} V_{sg}$ (Zhu et al., 2011), where α_{sg} is the coefficient of adsorption strain. Therefore, Eq. (12) can be expressed as:

$$\begin{aligned}\frac{\partial \varepsilon_s}{\partial t} &= \alpha_{sg} V_L Y_1 Y_2 \\ &\quad \times\left\{\left[\frac{c_2 c_1 Y_3}{(1+c_2 p)^2} + \frac{1}{(p+p_L)^2}\right]\frac{\partial p}{\partial t} - \frac{c_1}{1+c_1 p}\frac{\partial T}{\partial t}\right\}\end{aligned} \tag{15}$$

In the conventional methane reservoir state, there is $\varepsilon_v + p/K_s - \varepsilon_S - \alpha_T T \ll 1$. Therefore, substituting Eq. (10) into Eq. (14) we can obtain:

$$\phi = \alpha - (\alpha - \phi_0)\exp(B - A) \tag{16}$$

where $A = \varepsilon_v + p/K_s - \varepsilon_S - \alpha_T T$, $B = \varepsilon_{v0} + p_0/K_s - \varepsilon_{S0} - \alpha_T T_0$.

Thus:

$$\frac{\partial \phi}{\partial t} = (\alpha - \phi)\left(\frac{\partial \varepsilon_v}{\partial t} + \frac{1}{K_s}\frac{\partial p}{\partial t} - \frac{\partial \varepsilon_s}{\partial t} - \alpha_T\frac{\partial T}{\partial t}\right) \tag{17}$$

Substituting Eqs. (15) and (17) into Eq. (13), we can obtain:

$$\begin{aligned}\frac{R}{M_g}Q_s &= \frac{1}{T_{ar}+T}\left[\phi + \frac{(\alpha-\phi)p}{K_s}\right]\frac{\partial p}{\partial t} \\ &\quad - \left[\frac{\phi p}{(T_{ar}+T)^2} + \frac{(\alpha-\phi)p\alpha_T}{T_{ar}+T}\right]\frac{\partial T}{\partial t} - \frac{1}{\mu}\nabla\left(\frac{pk}{T_{ar}+T}\right)\nabla p \\ &\quad + Y_1 Y_2 \times\left(\frac{p_a\rho_c V_L}{T_a} - \frac{(\alpha-\phi)p\alpha_{sg}V_L}{T_{ar}+T}\right) \\ &\quad \times\left\{\left[\frac{c_2 c_1 Y_3}{(1+c_2 p)^2} + \frac{1}{(p+p_L)^2}\right]\frac{\partial p}{\partial t} - \frac{c_1}{1+c_1 p}\frac{\partial T}{\partial t}\right\} \\ &\quad + \frac{p(\alpha-\phi)}{T_{ar}+T}\frac{\partial \varepsilon_v}{\partial t}\end{aligned} \tag{18}$$

The migration model for methane in coal seam containing the adsorption, heat transfer and stress effects is shown in Eq. (18). The fractal permeability can be obtained by Eq. (5).

2.2.2 Equations for thermal conductivity

Zhu et al. (2011) proposed the gradient of heat flux as:

$$\begin{aligned}\nabla\cdot\dot{q}_T &= -\nabla\lambda_M\nabla T - \lambda_M\nabla^2 T + \rho_g C_g\dot{q}_g(T + T_{ar}) \\ &\quad + C_g(T + T_{ar})\nabla(\rho_g\dot{q}_g) \\ &= -\lambda_M\nabla^2 T - (1-\phi)\lambda_s\nabla T - \lambda_g\nabla\phi\cdot\nabla T \\ &\quad + \rho_g C_g\dot{q}_g(T + T_{ar}) + C_g(T + T_{ar})\nabla(\rho_g\dot{q}_g)\end{aligned} \tag{19}$$

where $\dot{q}_T = -\lambda_M\nabla T + \rho_g C_g\dot{q}_g(T + T_{ar})$ is the total heat flux; C_g is the gas specific heat constant; and $\lambda_M = (1-\phi)\lambda_s + \lambda_g\phi$ is the heat conduction coefficient, where λ_s and λ_g are the thermal conductivities of rock and gas. According to the

energy conservation equation, the unit heat capacity is related to the heat flow as follows (Tong et al., 2010):

$$\frac{\partial[(\rho C)_M(T+T_{ar})]}{\partial t}+(T+T_{ar})K_g\alpha_g\nabla\dot{q}_g +(T+T_{ar})K\alpha_T\frac{\partial\varepsilon_v}{\partial t}=-\nabla\dot{q}_T \tag{20}$$

$$(\rho C)_M=\phi\rho_gC_g+(1-\phi)\rho_sC_s \tag{21}$$

where $(\rho C)_M$ is the specific heat capacity of coal, and $\alpha_g=1/T$ is the thermal expansion coefficient. C_g and C_s are the heat constants of gas and solid.

Combining Eqs. (17) and Eqs. (19)-(21), we can obtain:

$$\begin{aligned}&(\rho C)_M\frac{\partial T}{\partial t}-(T_{ar}+T)\left[K_g\alpha_g\nabla\cdot\left(\frac{k}{u}\nabla p\right)-K\alpha_T\frac{\partial\varepsilon_v}{\partial t}\right]\\&=\lambda_M\nabla^2T+\frac{\rho_{ga}pT_aC_g}{Pa\,(T_{ar}+T)}\frac{k}{u}\nabla p\nabla T+(\lambda_g-\lambda_s)(\alpha-\phi)\\&\times\left[\nabla\varepsilon_v+\frac{\nabla p}{K_s}-\alpha_T\nabla T-\frac{\varepsilon_LY_1Y_2}{p}\left(X\nabla p-\frac{c_2\nabla T}{1+c_1p}\right)\right]\nabla T\end{aligned} \tag{22}$$

where $X=c_1c_2pY_3/(1+c_1p)^2+Y_1$.

The thermal capacity of the coal matrix is much higher than that of gas in the fractures. Therefore, the heat transfer process is quite slow. The heat flex is conducted faster in the fractures, but it is extremely slow in the solids. The propagation of elastic stress can be regarded as spontaneous. The governing equations for the model are shown as Eq. (23):

$$\begin{cases}k=\dfrac{\beta^3}{12A_f}\dfrac{D_f(1-\cos^2\gamma\sin^2\theta)}{4-D_f}l_{\max}^4\\Gu_{i,kk}+\dfrac{G}{1-2\mu}u_{k,ki}-\alpha p_{,i}-K\alpha_TT_{,i}-K\varepsilon_{s,i}+f_i=0\\\dfrac{\partial\phi}{\partial t}=(\alpha-\phi)\left(\dfrac{\partial\varepsilon_v}{\partial t}+\dfrac{1}{K_s}\dfrac{\partial p}{\partial t}-\dfrac{\partial\varepsilon_s}{\partial t}-\alpha_T\dfrac{\partial T}{\partial t}\right)\\\dfrac{R}{M_g}Q_s=\dfrac{1}{T_{ar}+T}\left[\phi+\dfrac{(\alpha-\phi)p}{K_s}\right]\dfrac{\partial p}{\partial t}\\-\left[\dfrac{\phi p}{(T_{ar}+T)^2}+\dfrac{(\alpha-\phi)p\alpha_T}{T_{ar}+T}\right]\dfrac{\partial T}{\partial t}-\dfrac{1}{\mu}\nabla\left(\dfrac{pk}{T_{ar}+T}\right)\nabla p\\+Y_1Y_2\times\left[\dfrac{p_a\rho_cV_L}{T_a}-\dfrac{(\alpha-\phi)p\alpha_{sg}V_L}{T_{ar}+T}\right]\\\times\left\{\left[\dfrac{c_2c_1Y_3}{(1+c_2p)^2}+\dfrac{1}{(p+p_L)^2}\right]\dfrac{\partial p}{\partial t}-\dfrac{c_1}{1+c_1p}\dfrac{\partial T}{\partial t}\right\}\\+\dfrac{p(\alpha-\phi)}{T_{ar}+T}\dfrac{\partial\varepsilon_v}{\partial t}\\(\rho C)_M\dfrac{\partial T}{\partial t}-(T_{ar}+T)\left[K_g\alpha_g\nabla\cdot\left(\dfrac{k}{u}\nabla p\right)-K\alpha_T\dfrac{\partial\varepsilon_v}{\partial t}\right]\\=\lambda_M\nabla^2T+\dfrac{\rho_{ga}pT_aC_g}{Pa\,(T_{ar}+T)}\dfrac{k}{u}\nabla p\nabla T+(\lambda_g-\lambda_s)(\alpha-\phi)\\\times\left[\nabla\varepsilon_v+\dfrac{\nabla p}{K_s}-\alpha_T\nabla T-\dfrac{\varepsilon_LY_1Y_2}{p}\left(X\nabla p-\dfrac{c_2\nabla T}{1+c_1p}\right)\right]\nabla T\end{cases} \tag{23}$$

where $X=c_1c_2pY_3/(1+c_1p)^2+Y_1$.

Eq. (23) is the coupled multi-physics field model, where the interaction of gas pressure and coal seam temperature (Eq. (12)) with the adsorption-desorption effect (Eqs. (13), (18) and (22)) leads to changes in effective stress (Eq. (14)) and coal seam deformation. The generation of coal seam deformation causes a change in porosity, which in turn reacts on the gas pressure (Eq. (2)) and coal seam temperature (Eq. (22)). Further, gas pressure and coal seam temperature (Eq. (9)) contribute directly to coal seam deformation. There is also an interaction between gas pressure and coal seam temperature (Eqs. (18) and (22)). The process of permeability evolution and the multi-factor coupling process are shown in Figs. 1 and 2. Based on fractal theory, this model describes the mechanical deformation, adsorption-desorption effects, seepage and thermal conduction process during the migration of CBM, and analyzes the influence of the coal seam microstructure on the multi-field coupling process.

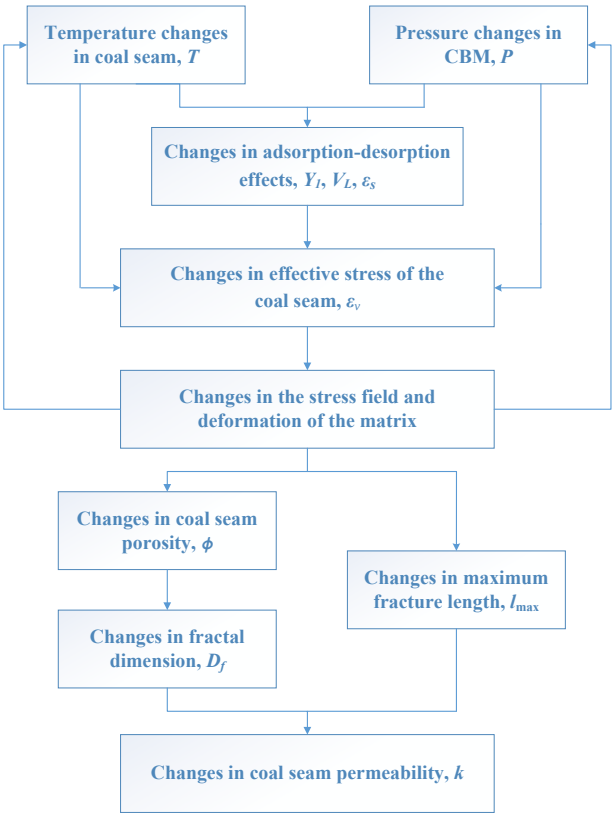

Fig. 1. Flow chart of permeability evolution.

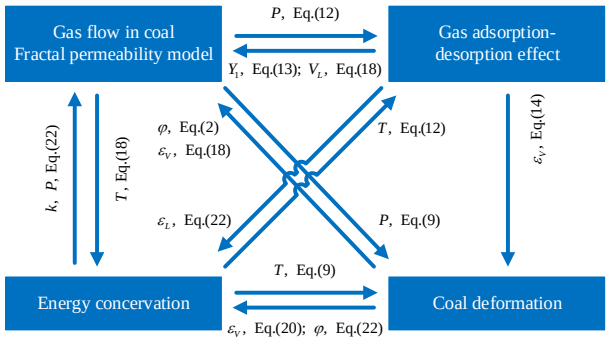

Fig. 2. The multi-factor coupling process.

Table 1. Parameters of coal seam and gas for the field case.

Parameter	Value
Young's modulus of coal, E (MPa)	2713
Young's modulus of coal grains, E_s (MPa)	4070
Poisson's ratio of coal, v	0.34
Density of coal, ρ_c (gm/cc)	1.52
Density of methane, ρ_g (kg/m^3)	0.717
Methane dynamic viscosity, μ (Pa·s)	1.84×10^{-5}
Langmuir pressure constant, P_L (psia)	280
Langmuir volume constant, V_L (scf/ton)	830
Porosity of coal, ϕ_0	0.3
Permeability of coal, k (mD)	0.7
Temperature, T(°F)	70
Volumetric thermal expansion of the solid, α_T (K^{-1})	2.4×10^{-5}
Thermal conductivity of coal, λ_S (J·/(m·s·K))	0.2
Specific heat capacity of coal, C_S (J·/(Kg·K))	1.25×10^{3}
Specific heat capacity of gas, C_g (J·/(Kg·K))	1.625×10^{3}

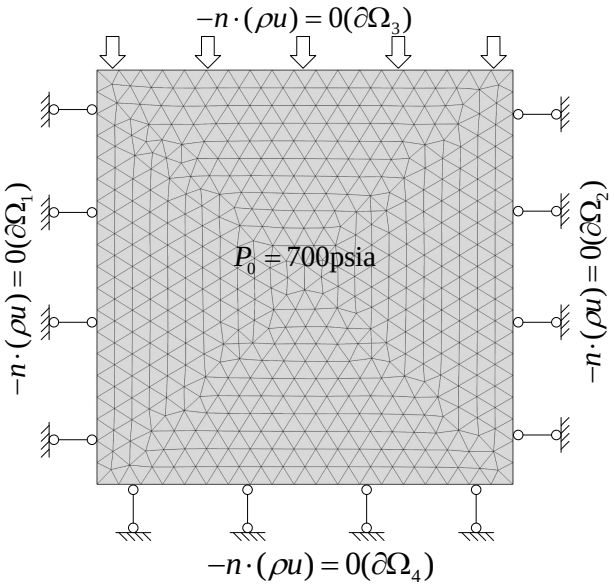

Fig. 3. Simulation model for verification.

3. Model verification against field data

In order to verify the reliability of the fractal multi-field coupled model proposed in this paper (Eq. (23)), we selected data from coal seam mining sites to develop a validation model, and thus proved the correctness of the fractal model. Most of the parameters were chosen from the experimental results (Ni et al., 2018), and unreported parameters were substituted from contemporary literature, as shown in Table 1. The dimension of the model simulation area is 568×568 m^2, and the boundary conditions and initial conditions of the model are shown in Fig. 3.

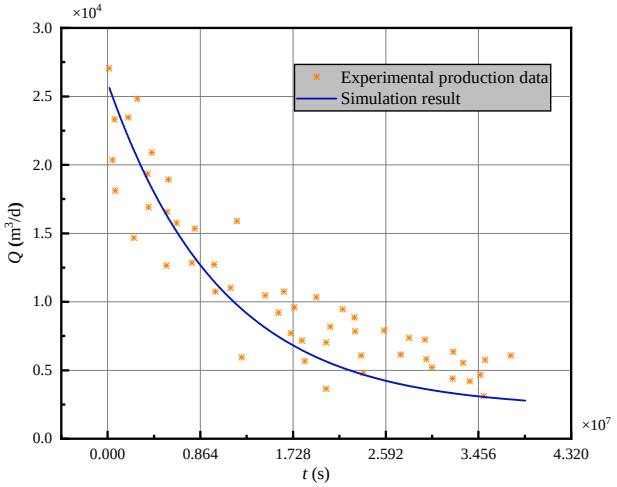

Fig. 4. Comparison of simulation results with field data on gas production.

Table 2. Parameters of coal seam and gas.

Parameter	Value
Young's modulus of coal, E (MPa)	2713
Young's modulus of coal grains, E_s (MPa)	4070
Poisson's ratio of coal, v	0.339
Density of coal, ρ_c (kg/m^3)	1.25×10^{3}
Density of methane, ρ_g (kg/m^3)	0.717
Methane dynamic viscosity, μ (Pa·s)	1.84×10^{-5}
Langmuir pressure constant, P_L (MPa)	1.57
Langmuir volume constant, V_L (m^3/kg)	0.043
Langmuir volumetric strain constant, ε_L	0.02295
Initial porosity of coal, ϕ_0	0.01
Initial permeability of coal, k_0 (m^2)	1×10^{-15}
Absolute reference temperature, T_0 (K)	300
Volumetric thermal expansion of the solid, α_T (K^{-1})	2.4×10^{-5}
Thermal conductivity of coal, λ_S (J·/(m·s·K))	0.2
Specific heat capacity of coal, C_S (J·/(Kg·K))	1.25×10^{3}
Specific heat capacity of gas, C_g (J·/(Kg·K))	1.625×10^{3}

The model (Eq. (23)) analyses various factors such as fracture deformation and thermal conduction. The temporal and spatial evolution of the flow is non-linear, and it is difficult to obtain an analytical solution. Therefore, we chose COMSOL Multiphysics to solve the partial differential coupled equations. The results compared with the experimental data on the natural methane production rate (Q) at different times (t) (Ni et al., 2018) are shown in Fig. 4. From these it can be concluded that the fractal model proposed in this paper agrees well with the coal seam mining site data.

4. Numerical experiments

The characteristic parameters of the coal seam matrix and methane are shown in Table 2. Most of the modelling parameters were from previous field and simulation experiments, and

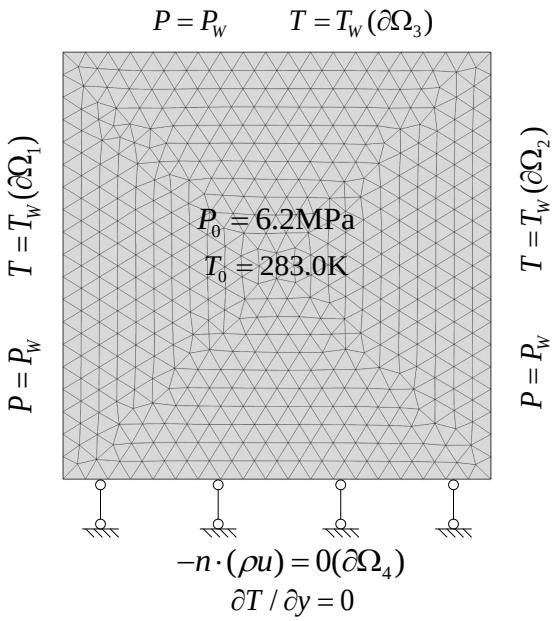

Fig. 5. Boundary and initial conditions of Scenario I.

those not reported in the table have been replaced by parameters from contemporary literature.

We applied two different simulation scenarios to illustrate the contribution of coal seam microstructure to thermal conductivity and methane seepage under the combined effects of ground stress, deformation and adsorption-desorption. These two scenarios are different stress states arising in the coal seam under different boundary condition. The first is the unconstrained plane strain state and the second is the uniaxial plane strain state. Based on these two scenarios in different states, we quantitatively analyzed the influence of coal seam microstructure on permeability, thermal conductivity effect and coal deformation during gas extraction. The evolution of the microstructural parameters of the coal seam was also analyzed. The processes described above are all considered the gas adsorption and the contraction effect of the coal seam matrix.

4.1 Scenario I: Thermal-seepage-deformation processes under unconstrained plane strain

In this scenario, we studied the migration of methane under unconstrained plane strain conditions. The geometry

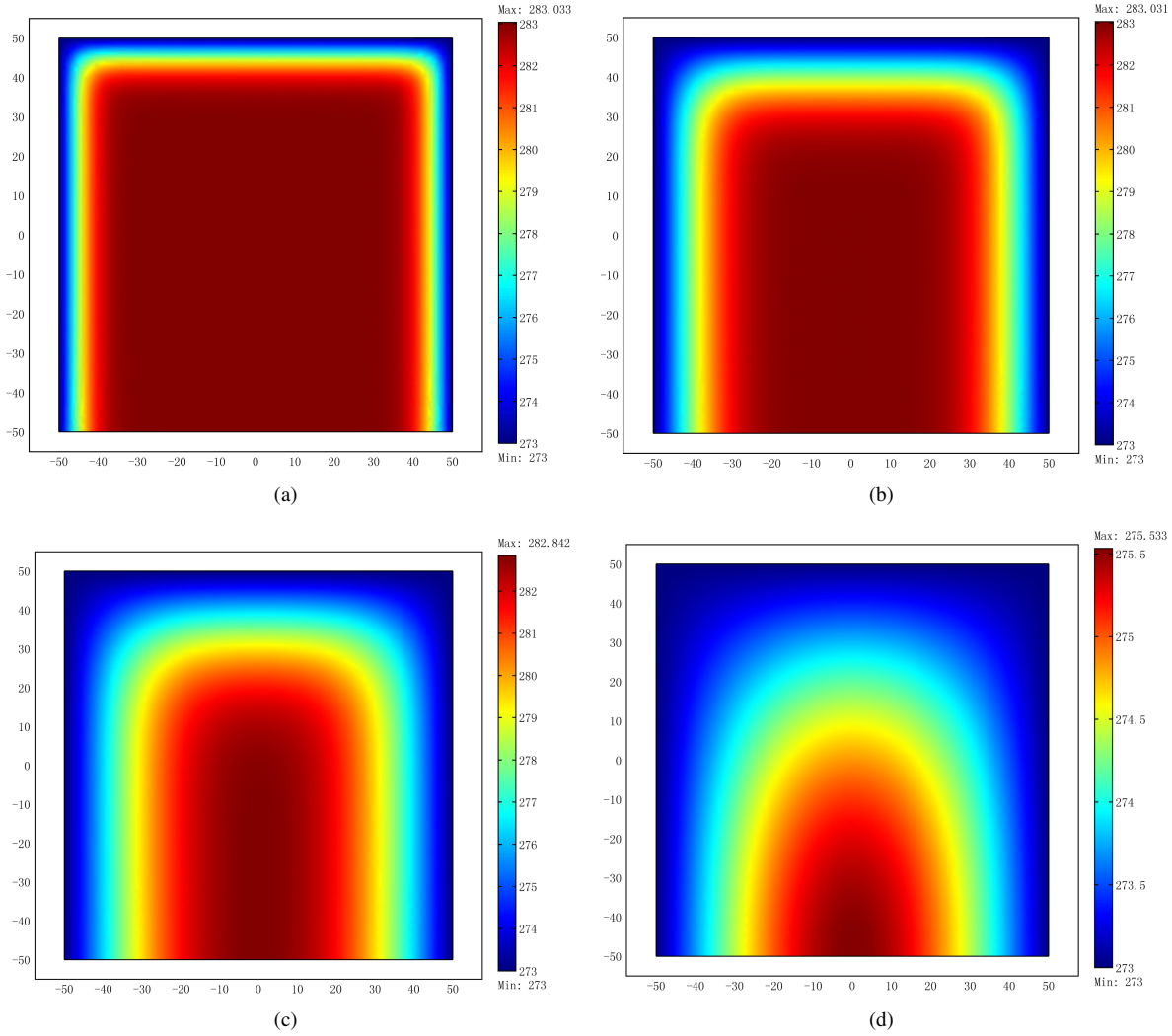

Fig. 6. Gas temperature distribution after (a) 1e8s, (b) 5e8s, (c) 1e9s, (d) 1e10s.

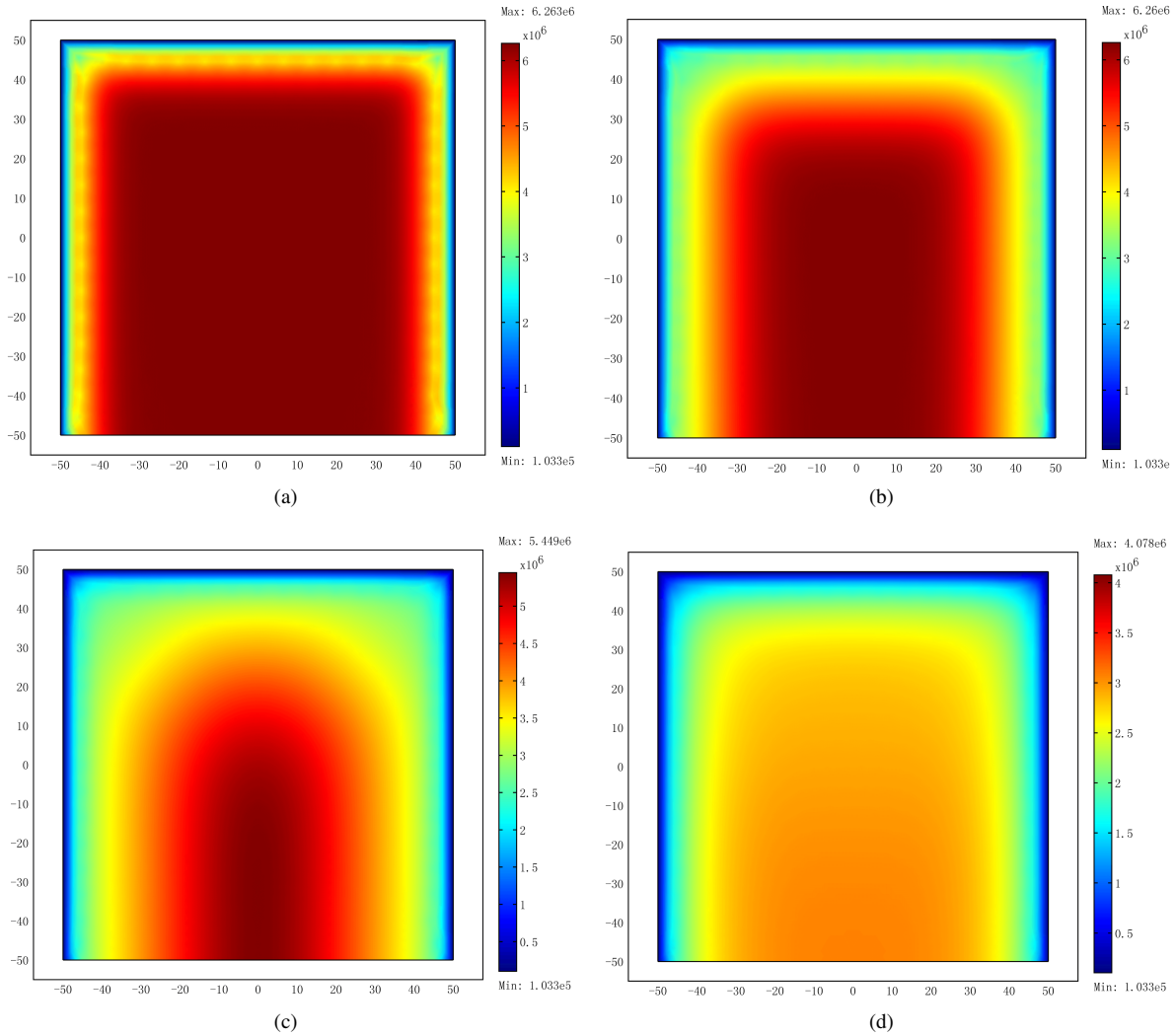

Fig. 7. Gas pressure distribution after (a) 1e8s, (b) 5e8s, (c) 1e9s, (d) 1e10s.

and boundaries of the simulation are shown in Fig. 5, for a rectangular area of 100×100 m constrained by the bottom only. This geometry has been used to describe the basic characteristics of gas migration in coal in previously published. The initial pressure of the coal seam is $P_0 = 6.2$ MPa, and the initial temperature is $T_0 = 283$ K. All three sides have an initial pressure of $P_w = 103.325$ kPa and an initial temperature of $T_w = 273$ K, except for the bottom side, which is thermally insulated with no gas flow.

With the seepage at stabilization, the temperature of the coal matrix at different mining times is shown in Fig. 6. It can be concluded with the continuation of the CBM mining process, there is an overall trend of coal body temperature decreases under the combined effect of adsorption and deformation extrusion under the ground stress. At the same time, due to thermal insulation, the temperature near the bottom edge does not change significantly. The highest temperatures occur in the middle and lower parts of the seam, and the high temperature zone gradually decreases as mining progresses.

The pressure distribution of the coal seam gas with the mining process is shown in Fig. 7. It can be concluded that the gas pressure decreases from the high-pressure zone in the middle of the seam towards the area with gas flow on three sides. At the same time, the extent of mining decompression continues to expand as mining proceeds.

With thermal conduction and seepage at stabilization, the stress distribution in the simulated area is shown in Fig. 8. As mining proceeds, the degree of model deformation gradually decreases. The bottom edge is a fixed constraint which limits the deformation of the coal seam. Under the effect of long-term mining, the coal matrix is regarded as a high stress zone, leading to the deformation of the coal matrix gradually increasing from the fixed end to the free end.

The multi-field coupled fractal model proposed in this paper is based on the microstructure of the coal seam. Thus, we have selected the two most significant structural parameters of the coal seam fracture: the fractal dimension for the fracture and the maximum fracture length (Liu et al., 2020). At the same time, we selected the classical cubic permeability equation applied in previously published models of thermal conduction seepage in coal seam:

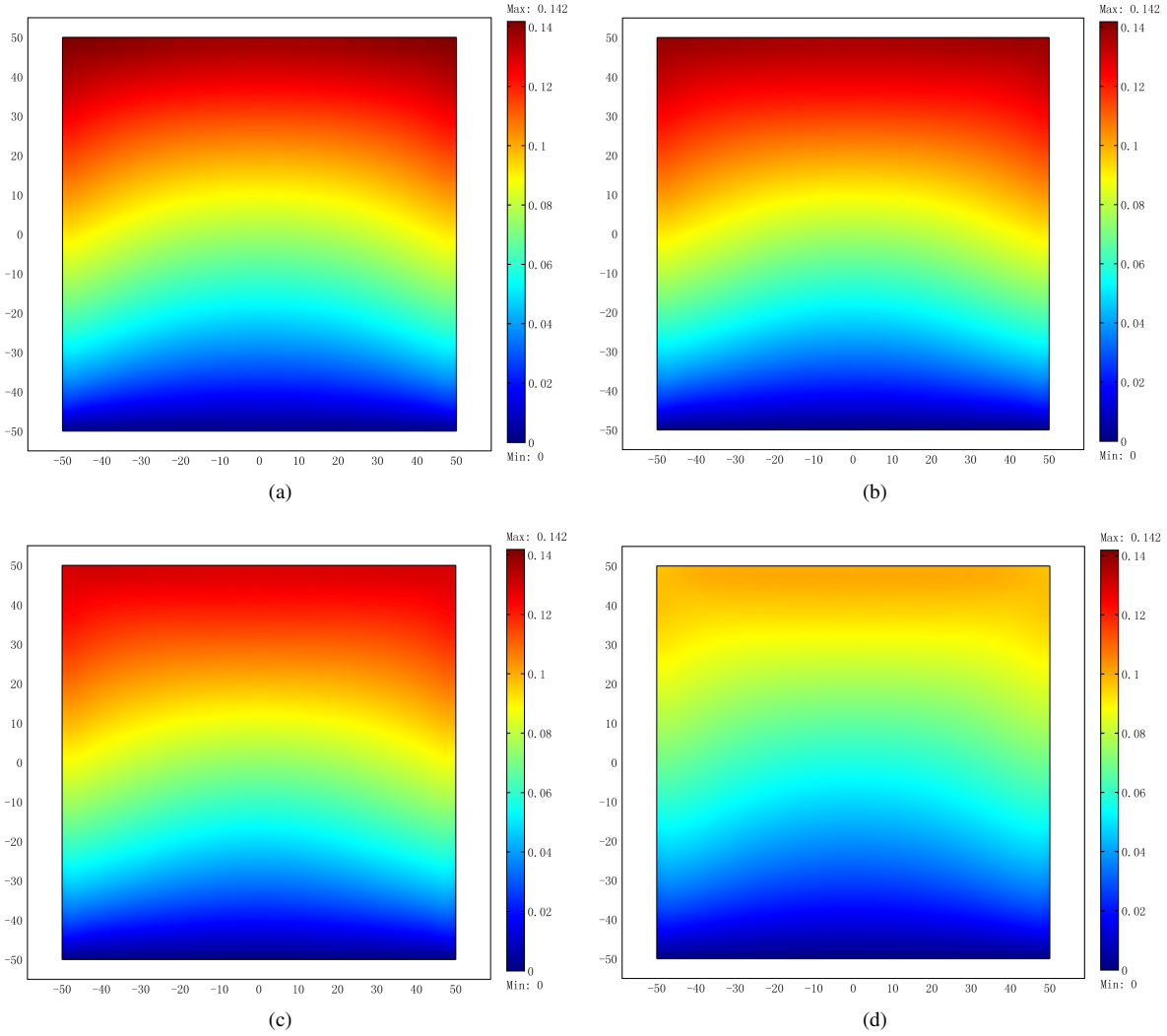

Fig. 8. Coal deformation distribution after (a) 1e8s, (b) 5e8s, (c) 1e9s, (d) 1e10s.

$$\frac{k}{k_0} = \left(\frac{\phi}{\phi_0}\right)^3 \tag{24}$$

where the porosity ϕ is obtained by Eq. (16).

We obtained the evolution of the permeability (m^2) with the fractal dimension of the fracture when the seepage and thermal conduction processes are stable. The comparison on the results of the classical cubic model and the fractal model is shown in Fig. 9.

It can be observed that the fractal dimension of the fracture has a significant effect on the permeability of the coal body. In particular, when the fractal dimension reaches 1.75, the coal seam permeability increases by 17.09% compared to the initial value. As the fractal dimension of the fractures increases, the coal seam fractures expand and many new, tiny fractures are created, leading to an increase in the permeability of the coal seam. However, previously published seepage thermal conductivity models do not take into account the microstructural characteristics of the coal seam and are therefore unable to draw these conclusions.

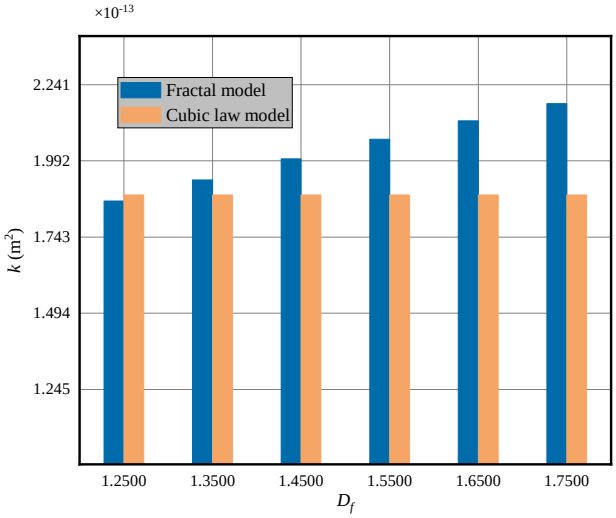

Fig. 9. Permeability evolution under the fractal dimension of the fracture.

In addition, we analyzed the contribution of another coal

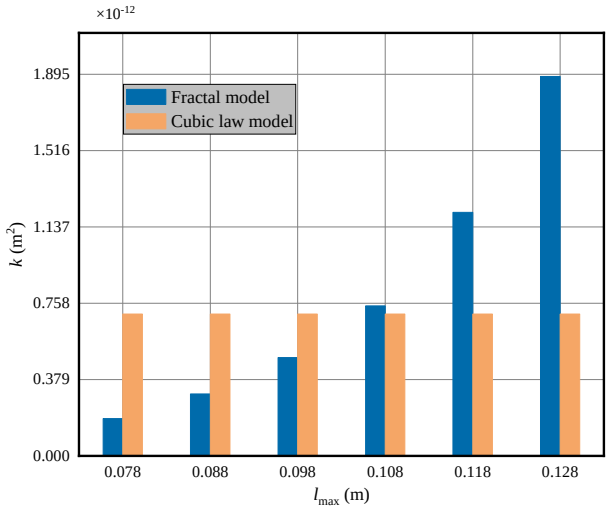

Fig. 10. Permeability evolution under the maximum length of the fracture.

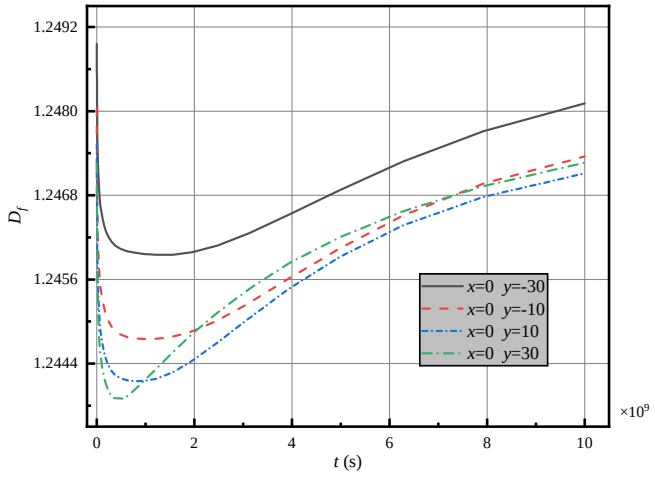

Fig. 12. Evolution of the fractal dimension at different positions.

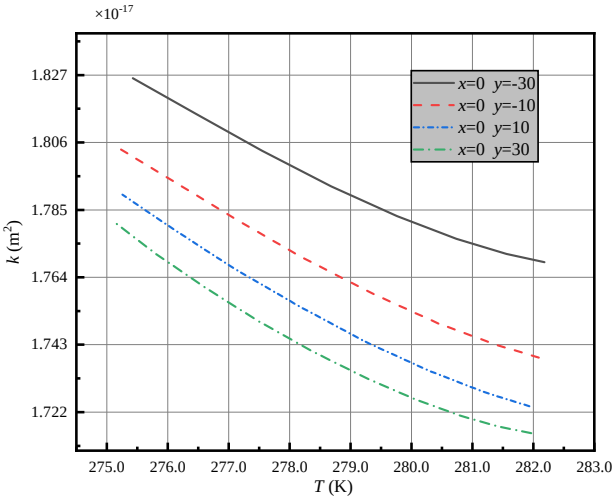

Fig. 11. Permeability evolution under different temperatures.

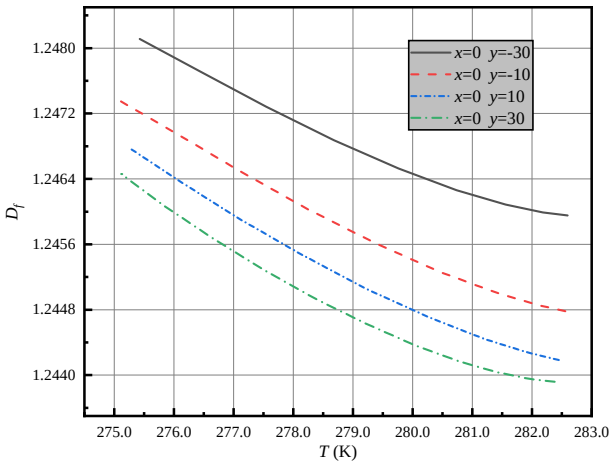

Fig. 13. Evolution of fractal dimension at different coal temperature.

seam structural parameter, the maximum fracture length (m), to the permeability of the seam, as shown in Fig. 10. It can be concluded that the maximum fracture length contributes significantly to the permeability of the coal seam. Compared with the cubic heat transfer model, the fractal model proposed in this paper is more realistic in characterizing the migration properties of methane. The increase in maximum fracture length characterizes the gradual increase of fractures in the coal seam under the effect of ground stress. As a result, gas flows more easily in the fractures, leading to a significant increase in permeability. In this case, when the maximum fracture length is 0.128, the coal seam permeability is enhanced by 91.56% from the initial permeability. Therefore, we found that the coal seam structure has a significant effect on gas seepage. Besides, the fractal model has significant advantages over the traditional cubic thermal seepage model.

The simulation results in this scenario are geometrically symmetrical due to the mechanical constraints of symmetry, and therefore we have chosen four monitoring points at equal distances from each other in the middle position $((0,-30),(0,-10),(0,10),(0,30))$. The evolution of the macroscopic permeability with the temperature at different locations is shown in Fig. 11. It can be concluded from Fig. 11 that with the increases in coal seam temperature, the permeability at different locations shows a decreasing trend. The permeability also decreases as the measurement location moves away from the fixed end. The trend also becomes progressively smaller. As the temperature rises, the gradual increase in coal seam deformation causes the original fractures to be squeezed shut, which is consequently detrimental to methane migration.

The evolution of the fractal dimension for different monitoring points is shown in Fig. 12. When the thermal conduction and the seepage process are stable, the overall fractal dimension of the coal seam tends to increase with the mining process, and the increase tends to become progressively slower. The fractal dimension reflects the complexity of the coal seam fractures. With the extraction of methane, numerous new fractures are gradually created in the coal seam under the

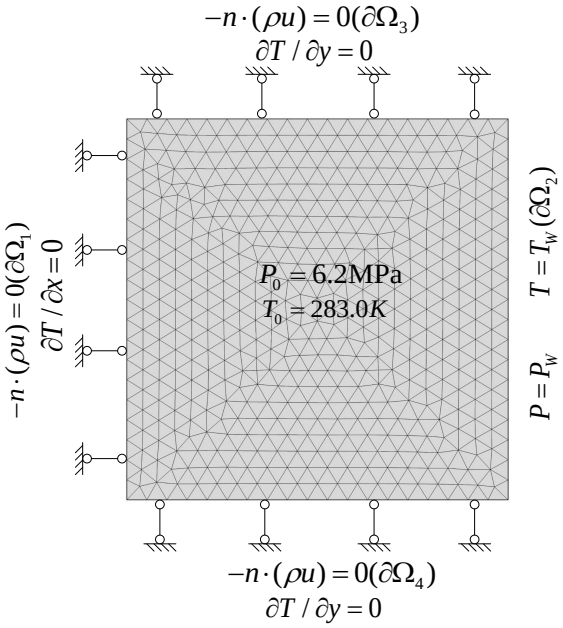

Fig. 14. Boundary and initial conditions of Scenario II.

long-term effect of high stress, resulting in a significant increase in the fractal dimension of the fractures.

We additionally analyzed the effect of coal seam temperature on the fractal dimension for the coal seam fracture, as shown in Fig. 13. In Fig. 13, the fractal dimension of the fractures at the different monitoring points decreases as the coal seam temperature increases. Concurrently, at the same temperature, the fractal dimension decreases as the monitoring point moves away from the fixed end. This is because, as the coal seam deformation increases with the temperature, more and more original fractures are squeezed closed, resulting in a decrease in the fractal dimension for the fracture.

4.2 Scenario II: Thermal-seepage-deformation processes under uniaxial stress conditions

This scenario illustrates the process of thermal conduction and seepage under uniaxial stress. The boundary conditions and initial values of the coal seam are shown in Fig. 14. This scenario applies the same geometry and material parameters as Scenario I, as shown in Table 1. Where the right side is free, while the other three sides are constrained by uniaxial

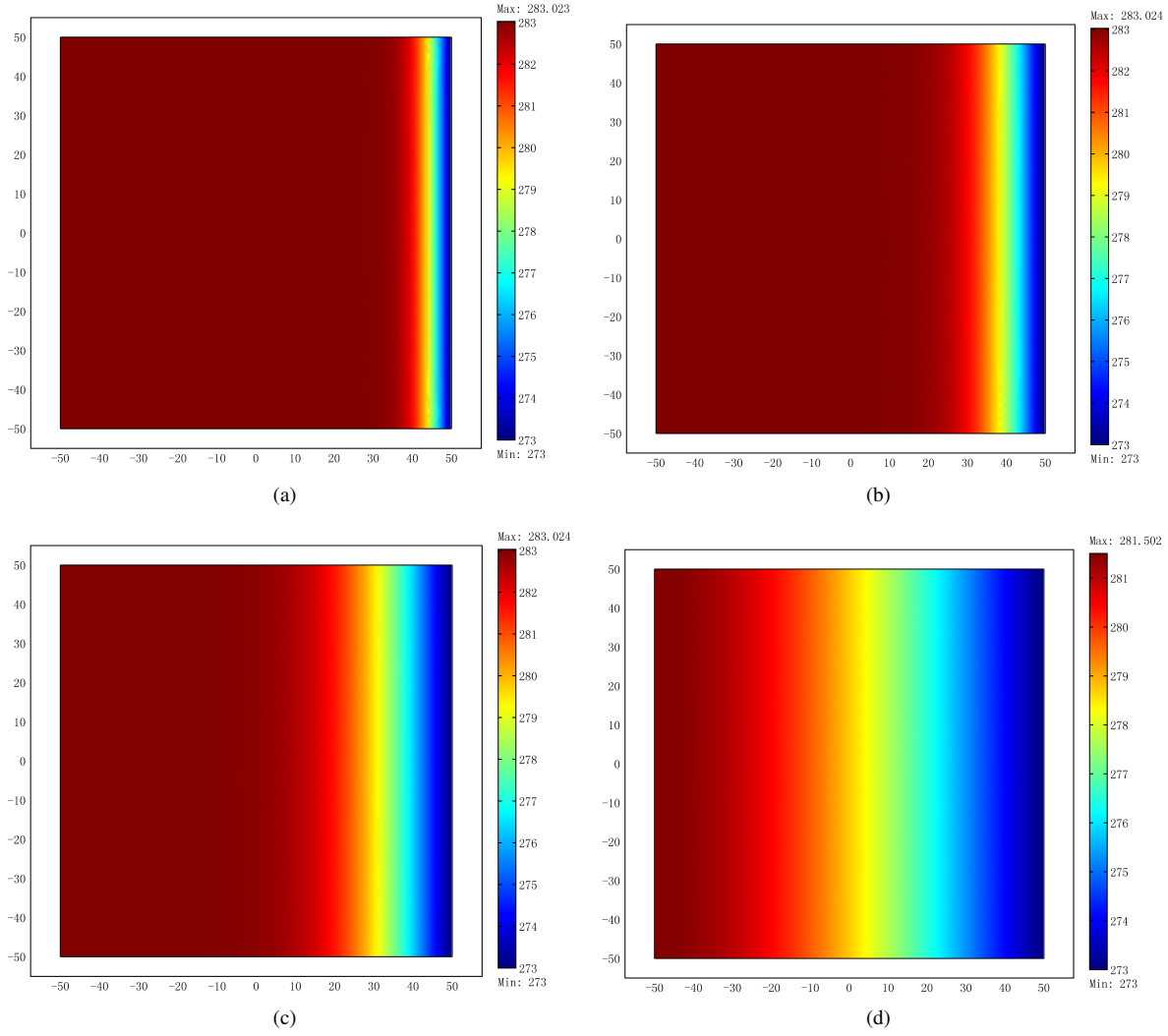

Fig. 15. Gas temperature distribution after (a) 1e8s, (b) 5e8s, (c) 1e9s, (d) 1e10s.

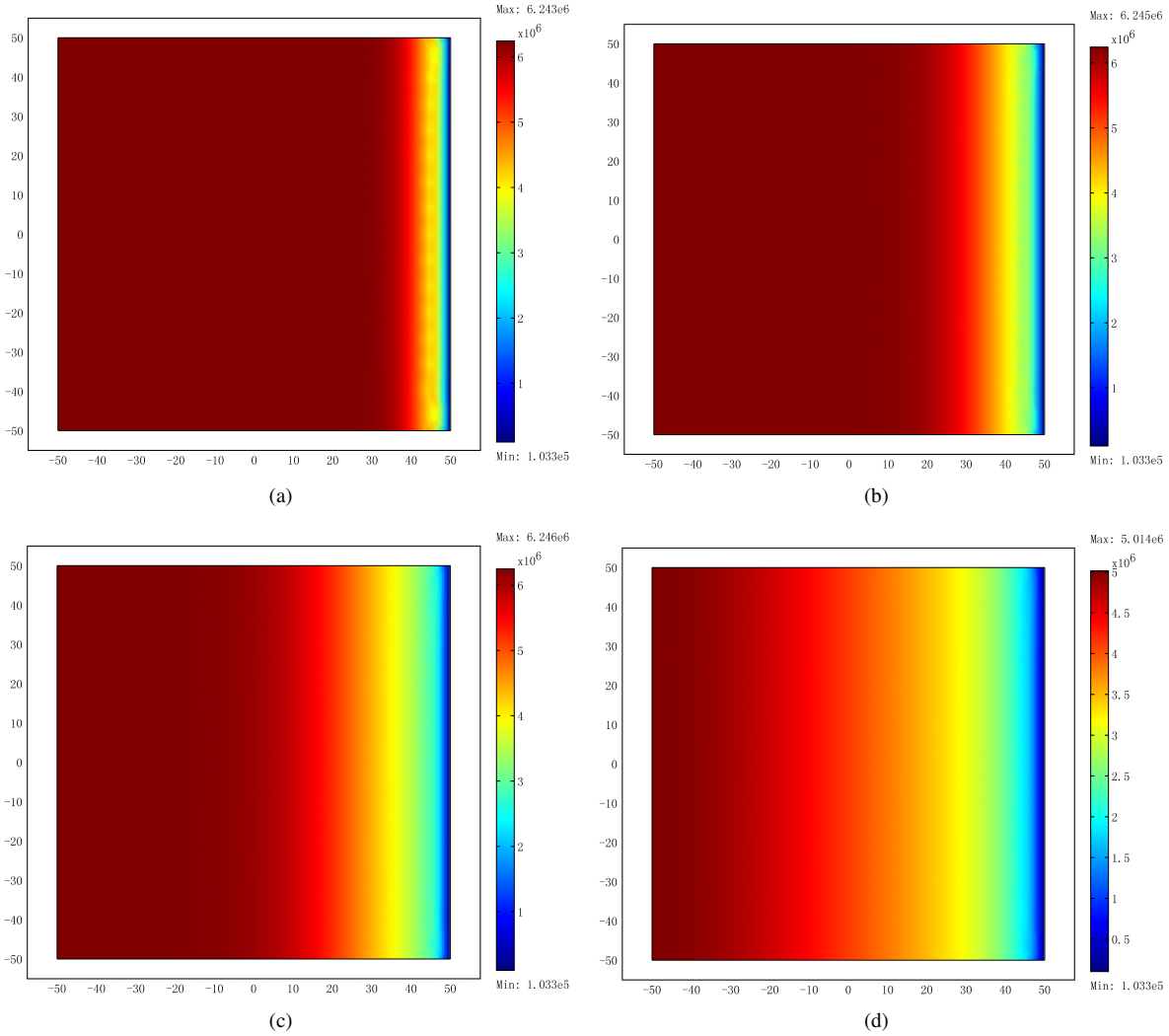

Fig. 16. Gas pressure distribution after (a) 1e8s, (b) 5e8s, (c) 1e9s, (d) 1e10s.

stress and no gas and heat exchange (zero fluxes).

The temperature distribution of the coal seam in Scenario II is shown in Fig. 15. We observe that the overall temperature of the coal seam shows a gradual decrease from left to right due to the gas fluxes only on the right side. The low temperature zone gradually expands under the combined effects of adsorption, deformation, and thermal conductivity.

The evolution of gas pressure with the extraction process for Scenario II is shown in Fig. 16. It can be concluded that the gas pressure distribution gradually decreases from the left side towards the extraction end (the right side) and the zone of the decrease gradually expands with the extraction process.

The stress distribution in the coal seam is shown in Fig. 17. The three constraint ends limit the deformation of the seam. As the mining of the coal seam progresses, the coal gradually deforms less from the free end to the fixed end. Also, the overall deformation of the seam increases with the duration of the mining.

We selected the two most important microstructural parameters of the coal seam: maximum fracture length and fractal dimension. The contributions of the structural parameters to the permeability (m^2) of the coal seam were also quantified. In addition, the classical cubic permeability model was compared with the fractal thermal conductivity model proposed in this paper to verify the advantages of the fractal model. The contributions of the fractal dimension and maximum fracture length (m) to the permeability are shown in Figs. 18 and 19.

It can be shown that the microstructural parameters of the coal seam have a significant influence on the permeability evolution of the seam. In particular, the fractal dimension of 1.75 increases permeability by 17.18% compared to the initial value (1.25). The maximum fracture length of 0.128 increases the permeability of the coal seam by 87.17% compared to the initial value (0.078). These conclusions cannot be drawn from previously published models which do not consider the microstructure of the coal seam. Coal seam structure has a significant impact on gas seepage, and the fractal model proposed in this paper is more applicable to the gas transport process.

Similarly, in this section we analyzed the evolution of the microstructure and characteristic parameters of the coal seam in Scenario II. It can be concluded from Figs. 14-17 that the

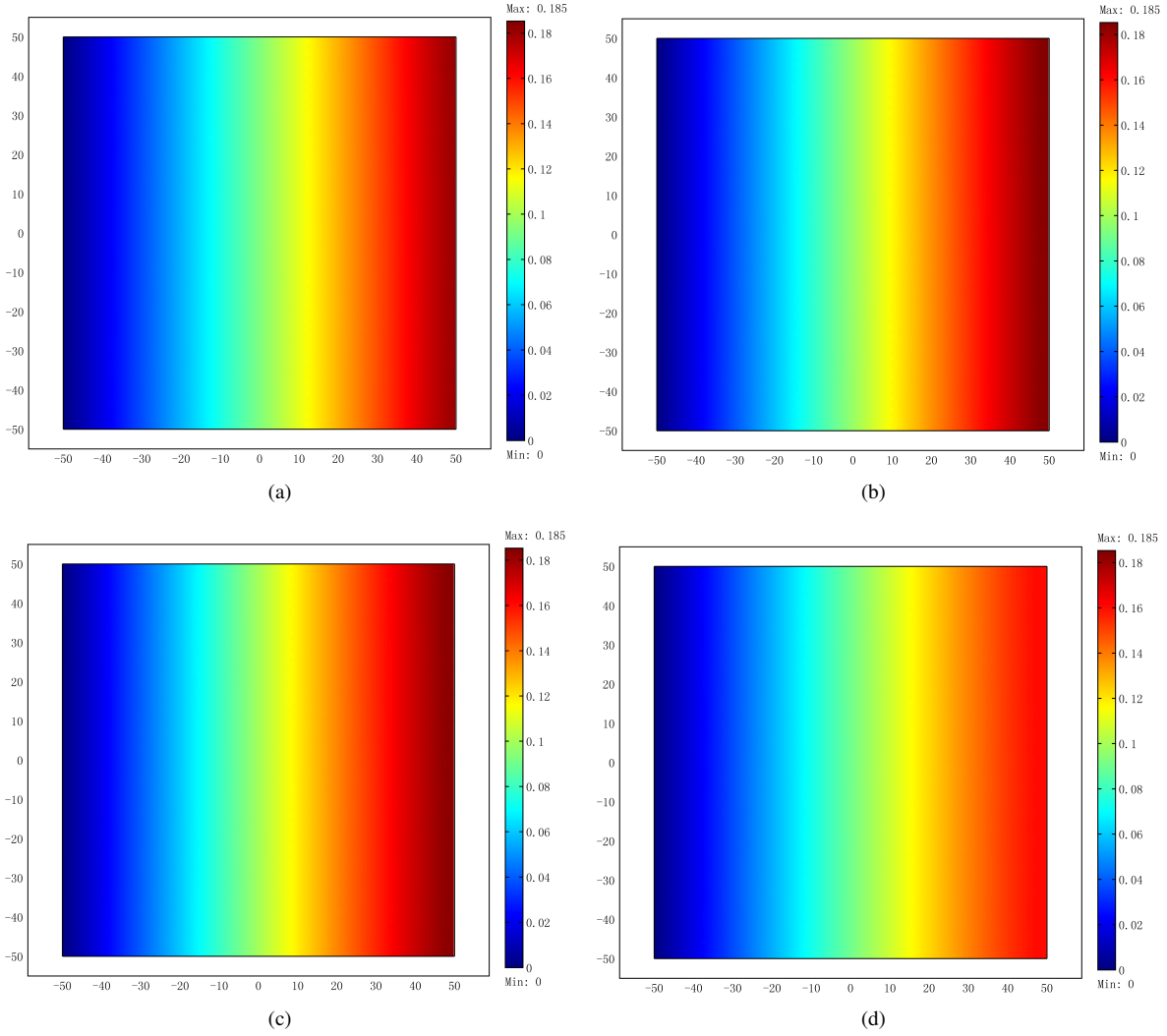

Fig. 17. Coal deformation distribution after (a) 1e8s, (b) 5e8s, (c) 1e9s, (d) 1e10s.

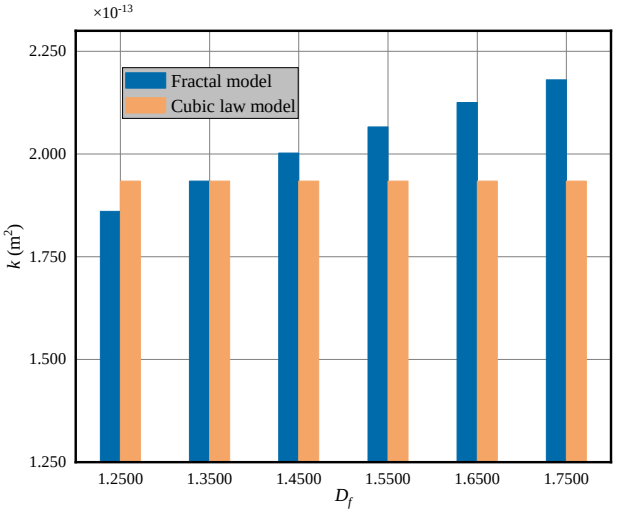

Fig. 18. Permeability evolution under the fractal dimension of the fracture.

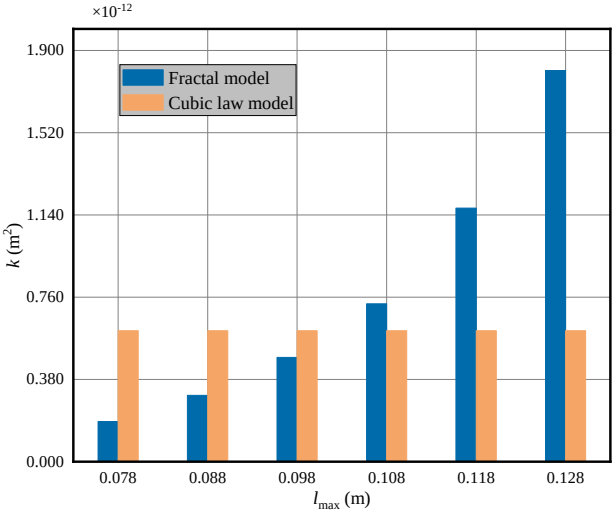

Fig. 19. Permeability evolution under the maximum length of the fracture.

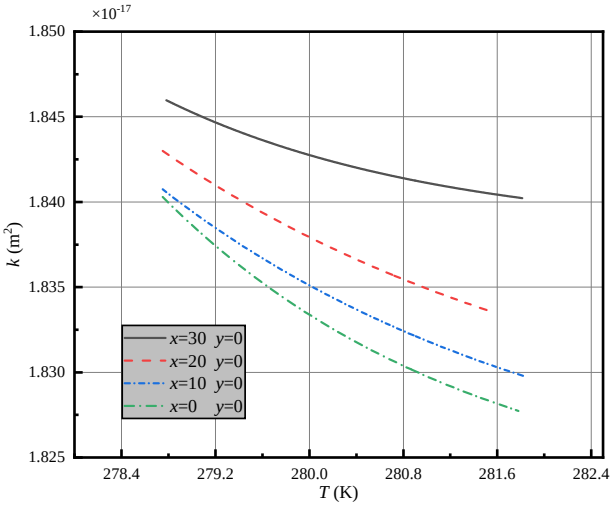

Fig. 20. Permeability evolution under different temperatures.

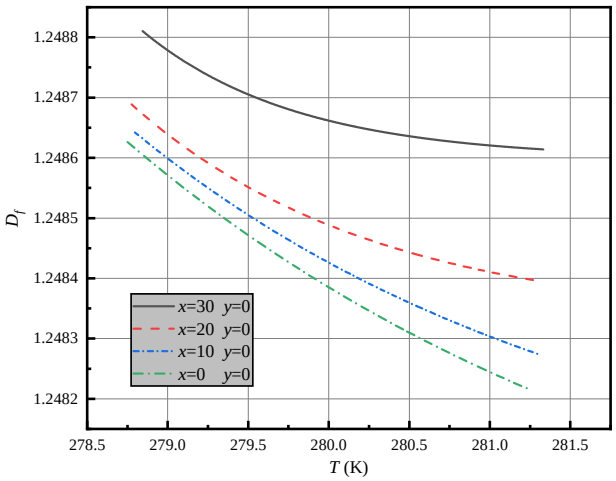

Fig. 22. Evolution of the fractal dimension at different coal temperatures.

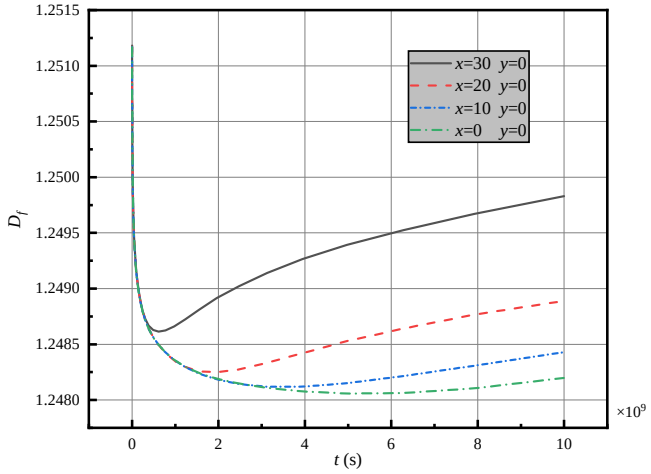

Fig. 21. Evolution of the fractal dimension at different positions.

results of simulation in this scenario are geometrically symmetric due to symmetric stress constraints. We therefore selected four equally spaced monitoring points with clearly distinguishable intermediate locations ((50, 50), (60, 50), (70, 50), (80, 50)). The permeability evolution of the coal seam with temperature at different locations is shown in Fig. 20. In Scenario II, the coal seam permeability tends to decrease overall with increasing temperature, which is consistent with the law of simulation results in Scenario I. At the same time, the permeability of the coal seam increases as the monitoring position gradually moves closer to the gas exchange end with the temperature unchanged.

In order to quantitatively analyze the evolution trend in the microstructure of the coal seam in Scenario II, we calculated the fractal dimension of the fracture at different locations in the mining process, as shown in Fig. 21. The overall fractal dimension in Scenario II tends to increase. As the mining process, new microfractures are created in the coal seam under the long-term effect of high ground stress, resulting in an increase in the fractal dimension. Additionally, the fractal dimension of the seam decreases as the location of the monitoring point moves away from the gas exchange edge (right boundary).

We also analyzed the effect of coal seam temperature on the fractal dimension at different monitoring locations, as shown in Fig. 22. We conclude from Fig. 22 that the fractal dimension at different locations decreases with increasing temperature, and the fractal dimension of the fracture increases when the monitoring point is located closer to the gas exchange end (right boundary)-when the seam temperature is the same. As the coal temperature increases, the coal matrix deformation increases, leading to fracture closure and a decrease in the fractal dimension.

5. Conclusion

In this study, we proposed a thermal-seepage-deformation model considering the microstructure of coal seam. This model quantifies the impacts of coal seam microstructure on thermal conduction, seepage and the matrix deformation. This study provides a new approach to analyzing the impact of coal seam microstructure on the reservoir gas migration. Based on the simulation results, we can conclude that:

- The microstructure of the coal seam is the principal component of gas from the unmined state to eventual equilibrium. Compared with previously published seepage models, the fractal model proposed in this paper provides a more realistic and reliable characterization of the resource migration and extraction processes in unconventional reservoirs.
- Coal seam permeability can be characterized by the two main coal seam microparameters: (a) the fracture fractal dimension, and (b) the maximum fracture length. Both structural parameters have significant effects on permeability under various extraction scenarios.
- For various extraction scenarios, the evolution of the structural parameters is approximately the same. The results show that both the fractal dimension and the permeability decrease with an increase of coal temperature. During the gas extraction process, the fractal dimension

of the fractures tends to increase gradually at different monitoring positions.

Acknowledgement

This work was supported by the Fundamental Research Funds for the Central Universities (No. 2020ZDPYMS02).

Conflict of interest

The authors declare no competing interest.

References

Arand, F., Hesser, J. Accurate and efficient maximal ball algorithm for pore network extraction. Computers & Geosciences, 2017, 101: 28-37.

Au, P. I., Liu, J., Leong, Y. K. Yield stress and microstructure of washed oxide suspensions at the isoelectric point: Experimental and model fractal structure. Rheologica Acta, 2016, 55(10): 847-856.

Barton, C. C., Hsieh, P. A. Physical and hydrologic-flow properties of fractures. Paper Presented at 28th International Geological Congress, Washington DC, 9-19 July, 1989.

Bustin, R. M., Clarkson, C. R. Geological controls on coalbed methane reservoir capacity and gas content. International Journal of Coal Geology, 1998, 38(1-2): 3-26.

Cai, J., Wei, W., Hu, X., et al. Fractal characterization of dynamic fracture network extension in porous media. Fractals, 2017, 25 (2): 1750023.

Cai, Y., Liu, D., Pan, Z. Partial coal pyrolysis and its implication to enhance coalbed methane recovery: A simulation study. Energy & Fuels, 2017, 31(5): 4895-4903.

Cui, X., Bustin, R. M. Volumetric strain associated with methane desorption and its impact on coalbed gas production from deep coal seams. AAPG Bulletin, 2005, 89(9): 1181-1202.

Durucan, S., Ahsanb, M., Shia, J. Q. Matrix shrinkage and swelling characteristics of European coals. Energy Procedia, 2009, 1(1): 3055-3062.

Harpalani, S., Schraufnagel, R. A. Shrinkage of coal matrix with release of gas and its impact on permeability of coal. Fuel, 1990, 69(5): 551-556.

He, J., Zhang, Y., Li, X., et al. Experimental investigation on the fractures induced by hydraulic fracturing using freshwater and supercritical CO_2 in shale under uniaxial stress. Rock Mechanics and Rock Engineering, 2019, 52(10): 3585-3596.

Jafari, A., Babadagli, T. Estimation of equivalent fracture network permeability using fractal and statistical network properties. Journal of Petroleum Science and Engineering, 2012, 92: 110-123.

Kulatilake, P., Shou, G., Huang, T. H., et al. New peak shear strength criteria for anisotropic rock joints. International Journal of Rock Mechanics and Mining Science & Geomechanics Abstracts, 1995, 32(7): 673-697.

Li W., Liu J., Zeng J., et al. A fully coupled multidomain and multiphysics model for evaluation of shale gas extraction. Fuel, 2020, 278: 118214.

Li, Z., Duan, Y., Fang, Q., et al. A study of relative permeability for transient two-phase flow in a low permeability fractal porous medium. Advances in Geo-Energy Research, 2018, 2(4): 369-379.

Liang, B. Study on temperature effects on the gas absorption performance. Journal of Heilongjiang Mining Institute, 2000, 10(1): 20-22. (in Chinese)

Liu, G., Liu, J., Liu, L., et al. A fractal approach to fully-couple coal deformation and gas flow. Fuel, 2019, 240: 219-236.

Liu, G., Ye, D., Gao, F., et al. A dual fractal poroelastic model for characterizing fluid flow in fractured coal masses. Geofluids, 2020, 2020: 2787903.

Liu, G., Yu, B., Gao, F., et al. Analysis of permeability evolution characteristics based on dual fractal coupling model for coal seam. Fractals, 2020, 28(7): 2050133.

Liu, G., Yu, B., Ye, D., et al. Study on evolution of fractal dimension for fractured coal seam under multi field coupling. Fractals, 2020, 28(4): 2050072.

McTigue, D. F. Thermoelastic response of fluid-saturated porous rock. Journal of Geophysical Research Atmospheres, 1986, 91(B9): 9533-9542.

Miao, T., Yang, S., Long, Z., et al. Fractal analysis of permeability of dual-porosity media embedded with random fractures. International Journal of Heat and Mass Transfer, 2015, 88: 814-821.

Miao, T., Yu, B., Duan, Y., et al. A fractal analysis of permeability for fractured rocks. International Journal of Heat and Mass Transfer, 2015, 81: 75-80.

Ni, X., Gong, P., Xue, Y. Numerical investigation of complex thermal coal-gas interactions in coal-gas migration. Advances in Civil Engineering, 2018, 2018: 9020872.

Øren, P. E., Bakke, S. Process based reconstruction of sandstones and prediction of transport properties. Transport in Porous Media, 2002, 46(2): 311-343.

Palmer, I. Permeability changes in coal: Analytical modeling. International Journal of Coal Geology, 2009, 77(1-2): 119-126.

Palmer, I., Mansoori, J. How permeability depends on stress and pore pressure in coalbeds: A new model. Paper SPE 36737 Presented at the SPE Annual Technical Conference and Exhibition, Denver, Colorado, 6-9 October, 1996.

Qin, X., Zhou, Y., Sasmito, A. P. An effective thermal conductivity model for fractal porous media with rough surfaces. Advances in Geo-Energy Research, 2019, 3(2): 149-155.

Raeini, A. Q., Bijeljic, B., Blunt, M. J. Generalized network modeling: Network extraction as a coarse-scale discretization of the void space of porous media. Physical Review E, 2017, 96(1): 013312.

Tong, F., Jing, L., Zimmerman, R. W. A fully coupled thermo-hydro-mechanical model for simulating multiphase flow, deformation and heat transfer in buffer material and rock masses. International Journal of Rock Mechanics & Mining Sciences, 2010, 47(2): 205-217.

Wang, D., Lv, R., Wei, J., et al. An experimental study of the anisotropic permeability rule of coal containing gas. Journal of Natural Gas Science and Engineering, 2018, 53: 67-73.

Wang, H., Xue, S., Shi, R., et al. Investigation of fault displacement evolution during extraction in longwall panel in an underground coal mine. Rock Mechanics and Rock Engineering, 2020, 53(4): 1809-1826.

Yu, B., Lee, L. J., Cao, H. A fractal in-plane permeability model for fabrics. Polymer Composites, 2002, 23(2): 201-221.

Yu, B., Li, J. Some fractal characters of porous media. Fractals, 2001, 9(3): 365-372.

Zeng, J., Liu, J., Li, W., et al. Evolution of shale permeability under the influence of gas diffusion from the fracture wall into the matrix. Energy & Fuels, 2020, 34(4): 4393-4406.

Zhang, H., Liu, J., Elsworth, D. How sorption-induced matrix deformation affects gas flow in coal seams: A new FE model. International Journal of Rock Mechanics and Mining Sciences, 2008, 45(8): 1226-1236.

Zhu, W., Wei, C., Liu, J., et al. A model of coal-gas interaction under variable temperatures. International Journal of Coal Geology, 2011, 86(2-3): 213-221.